Analysis of tire/road noise caused by road impact excitations

Peter Kindt, Filip De Coninck, Paul Sas, Wim Desmet
Department of Mechanical Engineering, Katholieke Universiteit Leuven, Belgium

ABSTRACT

This paper presents the experimental analysis of tire/road noise and tire vibrations during road impact excitations. The tests are performed on a setup which is based on a tire on tire principle. Radiated noise, vibrations of the tire surface and spindle forces are measured during impact excitations. The influence of driving speed, cleat dimension, inflation pressure, tire temperature and preload are analyzed. Two novel tire measurement techniques are presented for the validation and/or parameterization of tire models. Those techniques include the use of a 6 degree of freedom high frequency CUBE shaker table for the characterization of rotating and non-rotating tires up to 250 Hz.

INTRODUCTION

Tire/road noise generation mechanisms have been studied for several decades. The most influential mechanisms and related phenomena have been identified [1]. However, the relative importance of these mechanisms and phenomena for a certain operating condition of the tire is still under investigation. For instance, the influence of rolling on the tire modal parameters is not yet fully understood.

This research focuses on the tire/road noise caused by road impact excitations such as driving on cobbled roads, joints in a concrete road surface, railroad crossings, … The noise that is radiated from a tire strongly determines the passenger acoustic comfort and the traffic noise. Besides the radiated noise, the spindle forces induce vibrations that generate noise in the passenger compartment. Typical for a road impact excitation are a short duration tactile spike (shock) and a short duration noise spike (impact boom) experienced by a passenger. Even modern cars are sensitive to low frequency booming interior noise [2] when driving on rough roads.

In order to analyse the tire/road noise generating mechanisms during impact exaction, a test setup was designed and built at the K.U.Leuven vehicle technologies laboratory. The test setup is based on a tire on tire principle, which requires less space than a classic drum (rigid rotating cylinder). The setup performs highly repetitive and controllable impact excitation tests under various operating conditions. The experimental study of different influences factors on the tire impact response is based on a previously presented paper [3], and is extended to cover all major influence factors that a tire can experience. On the test setup, several parameters can be measured: radiated sound, vibrations of the tire surface and spindle forces. The tests presented in this paper focus on the spindle forces and vibrations of the tire surface due to impact excitations. The spindle forces and tire structural vibrations are the source of the structure borne and airborne tire/road noise, respectively. The presented analyses will contribute to the future development of a tire model to simulate the acoustic and structural response of a tire to road impact excitations.

TEST SETUP

In order to analyse the mechanisms of tire/road noise generation during road impact excitations, a novel test setup was designed and built. The test setup is based on a tire on tire principle, which makes the setup more compact and less expensive than a classic drum (rigid rotating cylinder). Moreover, the tire rolling deformation approaches better the deformation of a tire rolling on a flat road. The test setup performs highly repetitive and controllable impact excitation tests under various operating conditions.

The tires used in the tests are radial slicks (tires without tread pattern) of size 205/55R16 and the steel rims are rigidly clamped at the wheel hub. Figure 1 shows the test setup with the two tires mounted. Since two identical tires are used, the tire deformation of each tire is equal to the deformation of a tire rolling on a flat road (figure 2). One of the two tires is driven by a 7.5 kW, 8-pole, three-phase induction motor, while the other tire is mounted on a multiaxial wheel hub dynamometer with built-in encoder (figure 3). The piezo-electric dynamometer measures the three spindle forces and the three spindle moments. The x, y and z direction (figure 1) correspond to the longitudinal, lateral and vertical direction, respectively. The moments are defined as positive if their vector is pointing in the same direction as the force reference system defined in figure 1. The dynamometer has a measurement range of ±15 kN

and ±2500 Nm for the spindle forces and moments, respectively. The encoder in the dynamometer has a resolution of 144 pulses per revolution, which allows accurate measurements of the rotation speed.

The motor has 8 poles which limits the rotation speed to 750 rpm and yields low noise emission of the motor at normal operating conditions. The tire is directly mounted on the motor spindle and the rotation speed is controlled by a variable frequency drive. To simulate an impact on the tire, an aluminium cleat is guided through the contact area of the two tires. The cleat is mounted on the driven tire and can easily be replaced by a cleat with other dimensions. After installing the cleat, the tire is balanced to eliminate unbalance forces. As the cleat passes through the contact area of the two tires, the cleat is indenting both tires. This deformation is similar to the one of a tire rolling over a cleat with half the size of the cleat of the test setup. For example, when a circular cleat of diameter 10 mm is used in the test setup, both tires will deform as if they were rolling over a 5 mm semi-circular cleat on a flat road.

During all tests, the distance between the two tire spindles was fixed at 600 mm, which means that the static tire deformation of 16 mm did not change. The tire temperature was monitored by an infrared thermometer and kept constant at 25°C. The spindle forces and moments due to a cleat impact were measured at a sample frequency of 2048 Hz. The entire test setup is designed to avoid structural resonances below 750 Hz.

DYNAMIC SPINDLE FORCES

A series of tests were performed with different driving speeds, cleat dimensions, inflation pressures, tire temperatures and preloads. The spindle forces are compared in order to identify the generating mechanisms of structure borne tire/road noise during impact excitations. Moreover, the influence of the operating conditions on these generating mechanisms will be quantified. The Power Spectral Density (PSD) is used to analyse the spectral content of the signals. The spectra of several synchronous time blocks are averaged in the frequency domain. To do so, the force time signal is used to trigger the acquisition of a single impact. A series of single impact spectra is then used to calculate an averaged spectrum. In the tests, each spectrum is calculated out of 40 averages with a rectangular window.

DYNAMIC SPINDLE FORCES DUE TO CLEAT IMPACT

Figure 4 shows the longitudinal, lateral and vertical spindle force due to passing a 5 mm semi-circular straight cleat at 20.9 rad/s with an inflation pressure of 2.2 bar. The actual cleat in the test setup was a 10 mm circular cleat. The total vertical spindle force equals the sum of the static preload (2930 N) and the dynamic response force due to a cleat impact. All spindle forces shown in this paper are the dynamic forces due to a cleat impact.

Figure 4c shows that the vertical force F_z does not tend to decay to zero after the cleat impact. This is due to the geometrical unroundness (measured at 0.8 mm peak to peak) of the tire which causes a spindle force of approximately 150 N peak to peak at a frequency which is dependent on the rotation speed. Therefore a high-pass filter with cut-off frequency of 5 Hz was used to eliminate this force component. The power spectral density plot of each signal shows that the spectral content is limited to approximately 400 Hz. Above this frequency, the spectral content is negligible. The vertical force component F_z is the most important; therefore, the emphasis will be put on this force component. The vertical force F_z shows a damped oscillating pattern. The frequency of oscillation is 77.6 Hz, which corresponds to a distinct peak in the spectrum of figure 4c. This frequency is the (1,0) vertical resonance of the tire [4,5]. At this resonance, the belt translates as a rigid structure in the vertical direction.

At 220.7 Hz and 227.6 Hz appears a sharp peak in the spectrum of the longitudinal and vertical force, respectively. These frequencies are the longitudinal acoustic resonance f_l and the vertical acoustic resonance f_v of the air cavity [6]. The sharp peak indicates that the acoustic resonances are lightly damped. Figure 5 gives a schematic overview of the acoustic pressure distribution in the air cavity at resonance. This figure explains why the horizontal acoustic resonance is mainly observable in the horizontal spindle force spectrum of figure 4a.

Besides the above described spectral components, the response spectrum contains more, less dominant components. The measurement of rolling tire vibrations will provide more insight into the nature of these spectral components. The results of these measurements are described further in this paper.

INFLUENCE OF ROLLING SPEED

The influence of rolling speed on the tire structural resonance frequencies was described by Dorfi *et al.* [7]. The tire vibration modes of a non-rolling tire are similar to the modes of a rolling tire, however there is a resonance frequency shift when the tire goes from the non-rolling to the rolling condition. In order to analyse this phenomenon more in detail, a series of cleat impact tests were performed at different rolling speeds.

Figure 6 shows the spectra of the vertical spindle force at different speeds. The (1,0) vertical resonance, which has the most significant contribution to the spindle force response, appears at a slightly higher frequency as the rolling speed increases. Figure 7a shows the (1,0) vertical resonance frequency as a function of the rolling speed. The figure shows a significant drop in resonance frequency between the static and slow rolling tire. The deformation cycling of the rubber, as a result of the rolling, causes a softening effect [7] which explains the drop in resonance frequency. This effect is more pronounced for tires with a low aspect ratio and stiff sidewalls. After the onset of rolling, which causes the softening of the rubber, the graph shows an upward tendency. This is caused by the stiffening of the tire structure due to centrifugal forces. For this tire, the increase of the first vertical resonance frequency is approximately 2.4 Hz per 10 km/h increase of speed. Figure 7b gives the vertical and longitudinal acoustic resonance frequency as a function of the rolling speed. The longitudinal resonance frequency remains constant, while the vertical resonance frequency shows an increase. In this speed range, the same trend was observed by Yamauchi *et al.* [8]. The authors found that the longitudinal and vertical acoustic resonance frequency, respectively, decreases and increases with increasing driving speed. However, this effect is more distinct at speeds above 30 km/h.

INFLUENCE OF INFLATION PRESSURE

Figure 8 shows the spectrum of the vertical spindle force at different inflation pressures. The inflation pressure ranges from 1.7 to 2.7 bar, which are realistic values for the inflation pressure of a passenger car tire. To maintain the condition of identical tires in the test setup, both tires are inflated at the same pressure. The distance between the two tire spindles is fixed in this test, which yields a constant tire deflection at the different inflation pressures. As a result, the radial preload of the tire increases with rising inflation pressure. The legend of figure 8 gives for every inflation pressure the corresponding preload. As the inflation pressure increases, the spectrum shows in general a higher amplitude and a positive frequency shift at the structural resonances. This shift is caused by stiffening of the tire structure due to the higher inflation pressure. Both belt and sidewalls are stiffer suspended by the higher air pressure and experience a higher tension. The increased sidewall stiffness leads to an improved transfer of tire vibrations to the rim. The (1,0) vertical resonance frequency increases 6.9 Hz for a 1 bar inflation pressure increase. Other structural resonances also experience stiffening. However, the magnitude of the effect is dependent on the type of resonance. The spectra of the vertical spindle force show no noticeable change of damping due to inflation pressure variation.

The acoustic resonance frequencies experience no frequency shift. These frequencies are dependent on the geometry of the air cavity and the velocity of sound [5]. Equation 1 gives the speed of sound for an ideal gas, assuming that the sound wave causes an adiabatic compression [9].

$$c = \sqrt{\gamma \frac{p}{\rho}} = \sqrt{\gamma R T} \qquad (1)$$

The speed is dependent on the adiabatic index γ (1.402 for air), the pressure p and the density ρ. Using the ideal gas law, the speed of sound can be written as a function of γ, the gas constant of air R and the temperature T in Kelvin. This expression shows that both pressure and density contribute to the sound velocity equally, and in an ideal gas the two effects cancel out, leaving only the effect of temperature. As the acoustic resonance frequencies are invariant to the inflation pressure (figure 8), this indicates that also the geometry of the air cavity exhibits no significant change due to the inflation pressure variation. The static tire deflection in this test setup is constant as the distance between the two tire spindles is fixed. When a tire is mounted on a vehicle, the preload of the tire is constant and an increasing inflation pressure causes a decrease in static tire deflection. This change in deflection will cause a shift of the acoustic resonance frequencies. The inflation pressure affects also the “attack angle” (angle between the tyre circumference and the road at leading and trailing contact patch edge) and the contact area shape of a tire mounted on a vehicle.

INFLUENCE OF CLEAT HEIGHT

The dynamic behaviour of particle filled rubber strongly depends on the deformation magnitude, even for small deformations. With increasing deformation amplitude, the number of physical bonds in the filler network decreases, which results in a decrease of stiffness. This effect, which is known as the Payne effect [10], does not arise in unfilled rubbers. The tire tread compounds consist generally of carbon black or silica filled rubber. Consequently, the Payne effect might be of importance. In order to investigate this form of non-linearity in the tire response, a cleat test was performed with two different cleat heights.

Figure 9 shows the vertical spindle force spectra for a 5 mm and 7.5 mm high semi-circular cleat. The (1,0) vertical resonance shifts from 80.3 Hz to 78.1 Hz due to the increase of cleat height. The acoustic resonances are not subjected to a frequency shift because the acoustic cavity geometry is not changed by the higher excitation amplitude. Besides the frequency shift, the spectrum for the 7.5 mm cleat shows a clear peak at 115 Hz which corresponds to the (2,0) mode [5,6]. This mode involves two bending wavelengths in circumferential belt direction. The mode is less excited by the 5 mm cleat as shown in the spectra of figure 9. An operational modal analysis performed on the rotating tire at two different cleat heights showed that only the (1,0) resonance frequency shows a significant decrease [11]. At this resonance, the tire can be considered as a single degree of freedom system in which the rigid tire belt acts as a mass and the sidewalls provides stiffness and damping. This indicates that mainly the sidewall stiffness shows an excitation amplitude dependency.

INFLUENCE OF TIRE TEMPERATURE

It is known that material properties of viscoelastic materials can be strongly temperature dependent. A study of the temperature effect on tire/road noise showed that the noise emission for low frequencies (below 500Hz) and high frequencies (1.6 kHz up to 5 kHz) is affected by temperature [12]. On a bituminous pavement, the decrease in tire/road noise can exceed -0.1 dB(A)/°C. It was suggested that the effect of temperature for the low frequency noise is due to a reduction in tire stiffness which causes smaller contact forces. However, this was not further investigated. In order to verify the influence of temperature onto tire stiffness, a cleat impact test was performed at three different tire temperatures. The rotating tire was heated with electric radiative heaters in the vicinity of the rotating tire. The measurement was started when a stable equilibrium temperature of the rotating tire was reached. The tire inflation pressure was kept constant at 2.2 bar for the different tire temperatures. Due to the rather poor thermal conductivity of the rubber, the tire needed a considerable time to reach a thermal equilibrium. The temperature of the rotating tire surface was measured with an infrared thermometer. Figure 10 shows the spectrum of the vertical spindle force at three different temperatures. As the temperature increases, a decrease of the resonance frequencies can be noticed. For the first structural vertical resonance, a decrease of 0.12 Hz/°C in resonance frequency is found. Unlike the tire structural resonances, an increase of resonance frequency with increasing temperature is found for the acoustic resonances. The first acoustic natural frequency f of an unloaded tire can be calculated as a function of the speed of sound c and the median circumferential length L_c of the tire air cavity [6]:

$$f = \frac{c}{L_c} \qquad (2)$$

Based on equation (1) and (2), the temperature dependency of the acoustic resonance frequency is calculated at +0.16 %/°C in the temperature range of interest. This resonance frequency dependency is measured at +0.11 %/°C for the vertical acoustic resonance at 227 Hz. The horizontal acoustic resonance frequency will be subjected to the same temperature dependency. The difference between the calculated and measured dependency can be caused by the air temperature inside the tire which is lower than the measured tire surface temperature.

INFLUENCE OF PRELOAD

Figure 11 shows the power spectral density of the vertical spindle force for three different levels of preload. The inflation pressure was kept constant at 2.2 bar. The vertical resonance at 80 Hz shows a decrease in resonance frequency with increasing preload.

The analytical expression for the acoustic resonance frequencies of a loaded tire [6], shows that the vertical and horizontal acoustic resonance frequencies, respectively increase and decrease with increasing static deflection. The peak at 227 Hz in figure 11, which corresponds to the vertical acoustic resonance, shows a positive frequency shift. This confirms the deflection dependency of the acoustic resonances predicted by the analytical expression.

ROLLING TIRE VIBRATIONS

The mechanisms of tire noise generation can be classified into three main groups [1]. The first group are the whole tire vibrations which are caused by the road roughness and running deflection. These vibrations are important in the frequency band below 500 Hz. The second group are the tread block radial and tangential vibrations. The last group are the aerodynamic phenomena such as air pumping and tread groove resonances. The last two phenomena are important above 1000 Hz. This paper focuses on the radiated noise due to whole tire vibrations caused by road impact excitations. Therefore a smooth tire is used to eliminate the effect of the tread block vibrations and tread groove resonances.

The previous section showed that the vibration behaviour of a rolling tire is different than that of a

non-rolling tire. The rolling causes non-linear effects which are not observable on a non-rolling tire. Therefore, the analysis of the vibrations is performed on a rolling tire. The rolling tire vibrations are measured by means of a single point Laser Doppler Vibrometer (LDV) which allows contactless vibration velocity measurements. Figure 12 shows the setup to measure the radial component of the rolling tire vibrations. To measure the tread vibration, a plane mirror was used to reflect the laser beam in such a way that the laser perpendicularly irradiates the tire surface. The mirror is mounted on a support which can be considered as rigid in the frequency range of interest. The mirror support can be fixed at different locations around the tire, allowing a circumferential measurement resolution of 10°. The sidewall rolling tire vibrations are measured directly without reflecting the laser beam. The vibration measurements are performed with respect to a fixed reference frame because then the response can be used directly to perform a sound radiation analysis.

Figure 13 shows the measurement grid in which points are located on two circumferential rings on the tire tread and on one ring on the sidewall. The circumferential resolution is 10°. The vibration velocity normal to the tire surface is measured in each point of the grid.

ROLLING TIRE VIBRATION SPECTRA

Figure 14 shows the power spectral density of the average vibration velocity of the tread and the sidewall due to a 5mm semi-circular cleat impact excitation. The inflation pressure and preload are 2,2 bar and 2930 N, respectively. Comparison between the spectral density of the tread and the sidewall (fig. 14a) shows that the sidewall dynamic behaviour is dependent on the tread dynamic behaviour. The spectral content of the vibration velocity is limited to approximately 300Hz. In this frequency band, the level of tread vibration velocity is significant higher than the sidewall vibration level. However, the sidewall vibration level is higher in the frequency band from 300 till 800 Hz. The same trend was observed for a rotation speed of 17,0 km/h.

Figure 14b shows the averaged power spectral density of the tread vibration for two different rolling speeds. The higher rolling speed causes a higher vibration velocity level. Moreover, the spectral content of the vibration velocity differs significantly for the two tire rolling speeds. The spectral component at 81 Hz, which is dominant for the rolling speed of 28.3 km/h, is of less importance at 17 km/h. On the contrary, the spectral content of the spindle forces is less dependent on the tire rolling speed (fig. 6). Moreover, the acoustic resonances which contribute significantly to the dynamic spindle forces, show no important contribution to the vibration velocity response. Comparison between the average leading and trailing edge vibration velocity spectrum (fig. 15) shows that the dominant peaks match below 200 Hz. The vibration level of the leading edge is slightly higher than that of the trailing edge in this frequency band. The same trend was observed by other authors who analysed the sidewall rolling vibrations [13].

OPERATIONAL MODAL ANALYSIS

The above presented spectra of spindle forces and tire vibrations reveal several non-linearities of the rolling tire. Traditional modal analysis techniques are practically inapplicable to identify the dynamic behaviour of a rolling tire because the excitation forces are difficult measurable. However, operational modal analysis techniques allow the identification of the dynamic behaviour of a structure from the measured response only. The methods are based on the assumption of a flat excitation spectrum. As a result, harmonic components in the excitation force will be interpreted as structural resonances which have theoretically zero damping. The excitation caused by the cleat impact has a relative flat spectrum and is predominant compared to the excitation due to rolling of the tire. The method used in this paper is the Polyreference Least Squares Complex Exponential (Polymax) method applied to auto- and crosscorrelation functions. Under the assumption that the system is excited by white noise, correlation functions between the response signals can be expressed as a sum of decaying sinusoids [14]. Each decaying sinusoid has a damped natural frequency and damping ratio that is identical to that of a corresponding structural mode.

Comparison between the operational modal parameters of the rolling tire and the modal parameters of the non-rolling tire allows an assessment of the changes in dynamic behaviour due to rolling. Moreover, the operational modal analysis identifies the modes which are contributing to the cleat impact excitation response. The cleat impact response is measured in 58 points on the tread and 31 points on the sidewall. To maintain the phase relation between the different response points, the measurement of the vibration responses is triggered by the positive slope of the vertical spindle force. This approach requires a deterministic and highly repetitive spindle force signal, which is fulfilled for the impact measurements on the presented test setup. In order to reduce the influence of random noise, the vibration response due to the cleat impact is averaged in the time domain out of 40 averages. The crosspower spectrum between each response point and a chosen reference point is calculated and serves as an input for the operational modal analysis. The response chosen as reference should contain all of the relevant modal information, similar as is required

for the input reference location in a traditional modal test. The operational modal analysis results showed no noticeable coupling between the structural responses of the two tires.

Figure 16 shows the modal parameters of the rolling tire (17 km/h) excited by a semi-circular cleat of 5mm high. The mode shapes are depicted on the grid of figure 13b and for clarity, only the points on the tread are shown. The mode shapes resulting from an operational modal analysis technique are unscaled because the excitation is unknown. A mode can only be identified in the operational modal analysis if the mode is exited by the cleat excitation. Thus, every identified mode is contributing to the impact response. The identified modes are mainly modes which involve no rotation or bending of the belt in axial direction. This is due to the straight cleat used in this test, which excites the belt along the entire width. Modes above 200 Hz are difficult identifiable due to the limited excitation of the modes in this frequency band.

An interesting aspect of the operational modal analysis performed on the rotating tire is that clear standing wave patterns appear with respect to the fixed reference frame. A moving particle whose motion is described in a local reference frame that rotates with the tire is subjected to a Coriolis acceleration [15]. This causes the phase speed of the downstream and upstream going circumferential travelling waves in the local co-rotating reference frame to differ from each other. As a result, the down- and upstream going waves cannot interfere at a single natural frequency yielding a standing wave pattern. Additionally, in a fixed reference system, the circumferential phase speed of a downstream wave increases by the rotation speed, while for an upstream wave, the phase speed decreases by the same amount. However, the high damping makes it possible that there will be wave components propagating in opposite direction with the same wavelength at the same frequency, thus causing standing wave patterns. The identified modes from figure 16 are not perfectly real normal modes. Some mode shapes show nodal points which are not perfectly stationary and some points have a phase lag. This means that the modes show a degree of complexity. The same findings were reported by Tsujiuchi et al. [13].

Table 1 compares resonance frequencies and modal damping of a non-rolling tire [5,6] with those of a rolling tire at two different rolling speeds. The rolling tire resonances appear at lower frequencies compared to the non-rolling tire resonances. The frequency shift is in average 11% with a standard deviation of 2,22 Hz. The deformation cycling of the rubber, as a result of the rolling, causes a softening effect which explains the sudden drop in resonance frequency. After the onset of rolling, the resonance frequencies show no significant change as a function of rolling speed. The modal damping values show no dependency of the rolling speed.

NOISE RADIATION

Figure 17 compares the sound pressure level and the tire vibration velocity spectrum measured at the same tread point. The sound pressure was measured at a radial distance of 100mm from the tire surface. The sound pressure spectrum shows a dominant peak at 80,8 Hz which corresponds to the (1,0) vertical resonance. Besides this peak, also smaller peaks appear at the identified resonance frequencies of table1. Likewise the vibration velocity spectrum, the noise spectrum contains no pronounced contribution of the acoustic resonance frequencies. The spectral content of the radiated noise shows no important components at frequencies above 500 Hz. This indicates that the radiated noise due to a cleat impact is mainly caused by the whole tire vibrations. The radiated noise in the frequency range up to 500 Hz is not influenced by the tread pattern, but dependent only on the tire construction [16]. A sound intensity measurement is necessary to analyse the relation between vibration and sound radiation more in detail.
.

EXPERIMENTAL VALIDATION AND PARAMETERIZATION TECHNIQUES FOR TIRE MODELS

Numerical models are a powerful tool to study the behavior of a tire under specific conditions, be it static or dynamic. Because of its versatility and flexibility, the finite element method has become a common numerical simulation method. The accuracy of finite element models can be controlled by the number of degrees of freedom (level of detail), element formulations and material definitions. However, even very detailed and accurate tire models remain an approximation of reality. The challenge is to simplify this reality by creating approximated models that still allow simulating the structural behavior sufficiently well. During the modeling process, an analyst must deal with uncertainties on how to correctly model geometry, material properties, or boundary conditions. At the end of the modeling process, the accuracy of the model can be validated with experimental data.

The measurement techniques presented in this paper can be used either to validate a numerical tire model or to tune a model variable through a process of model updating. Typical model variables with high uncertainty are material parameters. In a detailed finite element model, every single component in the

tire structure is modeled and material properties are assigned to it. For simplified tire models, equivalent material properties are assigned to a part of the tire that consists of several components. For instance, the tire belt can be modeled in detail with all the different layers and their corresponding material properties. On the other hand, the belt can be modeled as a single layer with equivalent material properties. Those equivalent parameters should be chosen such that the behavior of the simplified structure describes the measured behavior. For most model updating procedures, experimental modal parameters are used. In this paper, two new experimental techniques are presented.

A first technique is the measurement of the dynamic stiffness of a non-rolling tire. The second technique determines the modal parameters of a rolling tire. Both measurements are performed with a CUBE high-frequency 6-DOF shaker table [17]. The shaker table has a control bandwidth of 0-300 Hz.

DYNAMIC STIFFNESS OF A NON-ROLLING TIRE

Figure 18 shows the test setup used for the measurement of the dynamic stiffness of a non-rolling tire which is fixed at the spindle. A piezo-electric 6 DOF dynamometer is attached to the shaker table surface. The shaker table provides a static preload and excites the tire through the dynamometer. The forces in the contact patch and the acceleration of the dynamometer table are measured. In the presented test, a random excitation signal in the frequency range 10 to 300 Hz is used to excite the tire in the z-direction. The shaker acceleration has a constant power spectral density of 0,1 $(m/s^2)^2/Hz$. In this setup, the force cell measurements must be compensated for the dynamic mass of the force cell platform. This dynamic mass was determined by measuring the force and acceleration of the force cell platform when the platform did not touch the tire. Figure 19 shows the amplitude and phase of the dynamic stiffness of the tire in z-direction. At the tire resonances, the dynamic stiffness shows a minimum in the amplitude. Because force and displacement are measured in the same point, an antiresonance appears between each pair of resonances. The vertical acoustic resonance at 227 Hz is also visible in the stiffness curve. Similar experiments could be repeated to determine the stiffness in x- and y-direction.

OPERATIONAL MODAL ANALYSIS OF A ROTATING TIRE

Two main problems are associated with an experimental modal analysis on a rotating tire. The first difficulty is to apply an excitation on the rotating tire which excites all modes in the frequency range of interest. The second problem is the excitation force measurement. This last problem can be overcome by using output-only methods. By assuming a flat excitation spectrum, modal parameters can be estimated from the responses only.

As shown in the previous chapters, a cleat excitation is a suitable excitation; however, modes above 200 Hz are hardly excited. In general, shaker excitation is more controllable than impact excitation which has limited frequency content. The presented setup uses the CUBE shaker capabilities to excite a structure in a controlled way. Figure 20 shows the setup in which one tire is mounted on the electric motor and the other tire is mounted on the CUBE shaker table. The shaker random acceleration in the z-direction has an RMS value of 16 m/s^2 in the frequency range 40 to 300 Hz. Because tire vibrations at higher frequencies are highly damped, a slope of +6dB/octave was used for the CUBE acceleration spectral density. Figure 21 compares time signal and spectral density of the measured vibration velocity for both types of excitation. Comparison of the time signals shows that the shaker excitation has a lower peak-to-RMS ratio which is more suited for the excitation of non-linear structures. The impact response is highly damped which accounts for a limited frequency resolution in the response spectra. The frequency resolution can be chosen much higher when using shaker excitation. The response spectrum obtained with the shaker excitation is much smoother at higher frequencies. It can also be seen that the acoustic resonances (peak at 225 Hz and 232 Hz) are better excited with the shaker.

CONCLUSION

The presented results show that the test setup performs highly repetitive and controllable impact excitation tests under various operating conditions. Although the test setup is limited to low speeds, the most important mechanisms and influences can be studied. The influence of rolling speed, inflation pressure, excitation amplitude, temperature and preload on the spindle forces was illustrated. The analyses of spindle forces and tire surface vibrations revealed a significant drop of the tire resonance frequencies at the onset of rolling. However, modal data is typical obtained from a non-rolling tire. This implies that the static modal test resonance frequencies are too high to predict an accurate rolling dynamic response. A tire model, based on modal parameters, should take into account this softening effect which is dependent on the tire construction.

The spindle force tests show an excitation amplitude dependency of the structural response which is caused by the non-linear sidewall stiffness. The acoustic resonances contribute significantly to the impact spindle force response and are independent of

the inflation pressure and excitation amplitude. In contrast, the acoustic resonances show no important contribution to the tire surface vibration response. An operational modal analysis identified the rolling tire resonances which contribute to the cleat impact response. Moreover, the influence of rolling on the dynamic behaviour of a tire was analysed.

The two presented new tire measurement methods which use the high frequency shaker table, allow the characterization of both a rotating and non-rotating tire up to 250 Hz.

ACKNOWLEDGMENTS

Research funded by a PhD grant of the Institute for the Promotion of Innovation through Science and Technology in Flanders (IWT-Vlaanderen).

REFERENCES

1. U. Sandberg, J. A. Ejsmont, Tyre/road noise reference book, Informex,Kisa, Sweden, 2002

2. M. Constant, J. Leyssens, F. Penne, R. Freymann, Tire and car contribution and interaction to low frequency interior noise, SAE 2001 Noise and vibration Conference; Traverse City, MI., 2001 May, SAE paper 2001-01-1528

3. P. Kindt, F. De Coninck, P. Sas, W. Desmet, Analysis of Tire/Road Noise Caused by Road Impact Excitations, SAE 2007 Noise and vibration Conference; St. Charles, Illinois, USA, 2007, May 15-17, SAE paper 2007-01-2248

4. H. R. Dorfi, A Study of the In-plane Force Transmission of Tires, Tire Science and Technology TSTCA, Vol.32, No. 4, Oct.-Dec. 2004, pp. 188-213

5. P. Kindt, F. De Coninck, P. Sas, W. Desmet, Experimental Modal Analysis of Radial Tires Under Different Boundary Conditions, The Thirteenth International Congress on Sound and Vibration ICSV13, Vienna, Austria, 2006 July 2-6, paper 223

6. P. Kindt, F. De Coninck, P. Sas, W. Desmet, Experimental modal analysis of radial tires and the influence of the tire modes on vehicle structure borne noise, 31st FISITA 2006 World Automotive Congress; Yokohama, Japan, 2006 Oct. 22-27, paper F2006D210

7. H. R. Dorfi, R. L. Wheeler, B. B. Keum, Vibration Modes of Radial Tires: Application to Non-rolling and Rolling Events, SAE 2005 Noise and vibration Conference; Traverse City, MI., 2005 May, SAE paper 2005-01-2526

8. H. Yamauchi, Y. Akiyoshi , Theoretical analysis of tire acoustic cavity noise and proposal of improvement technique, JSAE Review 23, 2002

9. P.M. Morse, K. U. Ingard, Theoretical acoustics, MC Graw-Hill Book Co., New York, 1968, pp.227-231

10. A. R. Payne, J. R. Scott, Engineering design with rubber, Interscience Publishers Inc., 1960, pp. 41-46

11. P. Kindt, P. Sas, W. Desmet, Measurement and Analysis of Rolling Tire Vibrations, Proceedings of the OPTIMESS2007 Workshop, 2007 May 28-30, Leuven, Belgium

12. F. A. Lédée, Y. Pichaud, Temperature effect on tyre-road noise, Applied Acoustics 68, 2007, 1-16

13. N. Tsujiuchi, T. Koizumi, A. Oshibuchi, I. Shima, Rolling Tire Vibration Caused by Road Roughness, SAE 2005 Noise and Vibration Conference, Traverse City, MI., 2005 May, SAE paper 2005-01-2524

14. LMS Test.Lab Operational Modal Analysis manual

15. Y.-J. Kim, J.S. Bolton, Effects of rotation on the dynamics of a circular cylindrical shell with application to tire vibration, Journal of Sound and Vibration 275, 2004, 605-621

16. E.-U. Saemann, J. Buschmann, J. Morkholt, Developments in Low Noise and Extended Mobility Tire Technology, 31st FISITA 2006 World

Automotive Congress; Yokohama, Japan, 2006 Oct. 22-27, paper F2006V064

17. F. De Coninck, W. Desmet, P. Sas, J. De Cuyper. Increasing the Accuracy of MDOF Road Reproduction Experiments: Experimental validation, SAE 2005 Noise and Vibration Conference, Traverse City, MI., 2005 May, SAE paper 2005-01-2393

CONTACT

e-mail: Peter.Kindt@mech.kuleuven.be

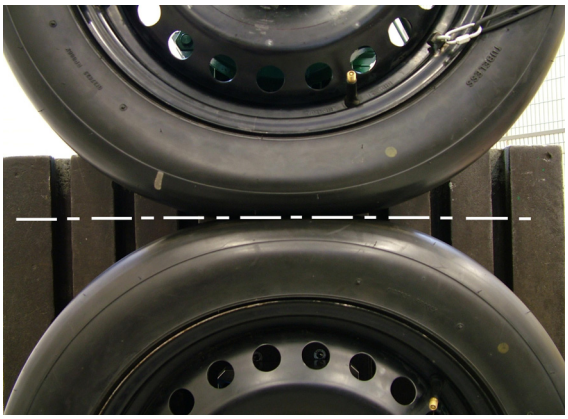

Fig.2: Static tire deformation in the test setup is identical as the tire deformation on a flat road.

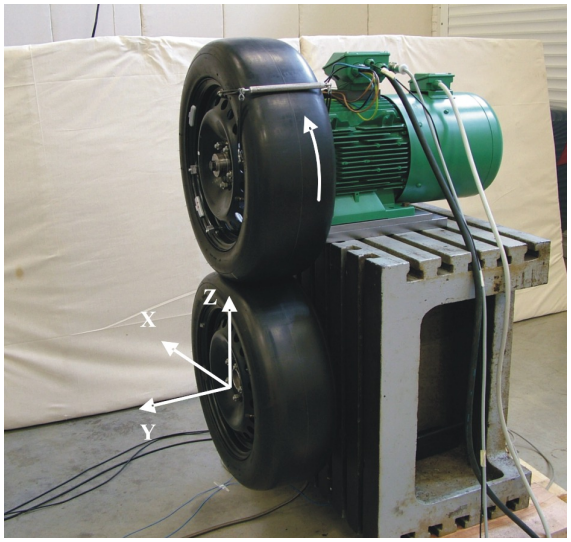

Fig.1: Test setup with two tires mounted.

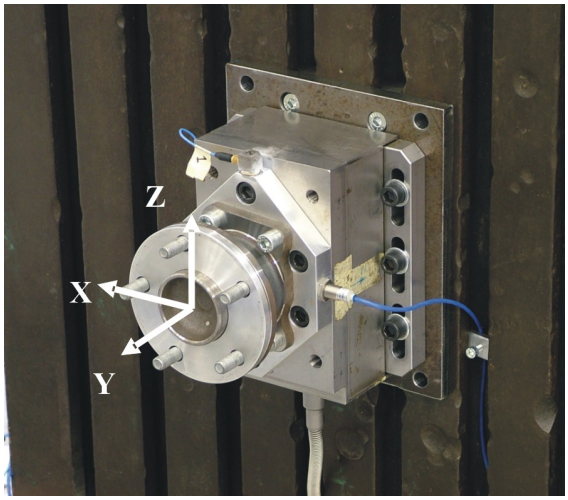

Fig. 3: Multiaxial wheel hub dynamometer with built-in encoder.

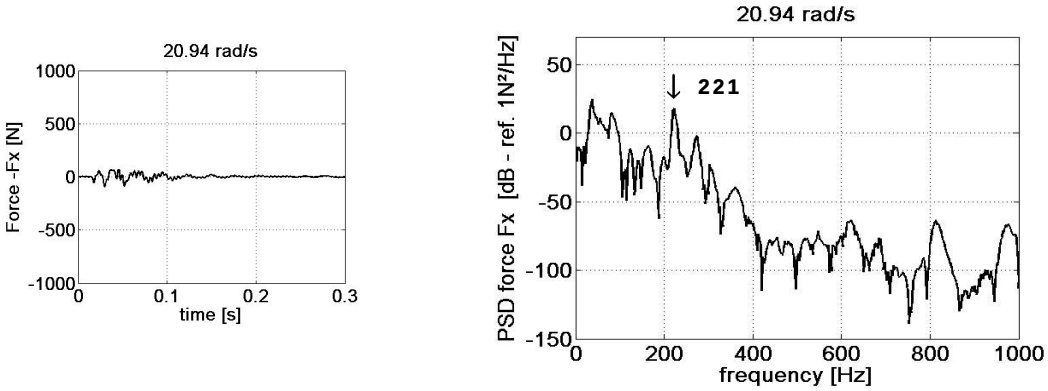

Fig. 4a: Longitudinal spindle force response

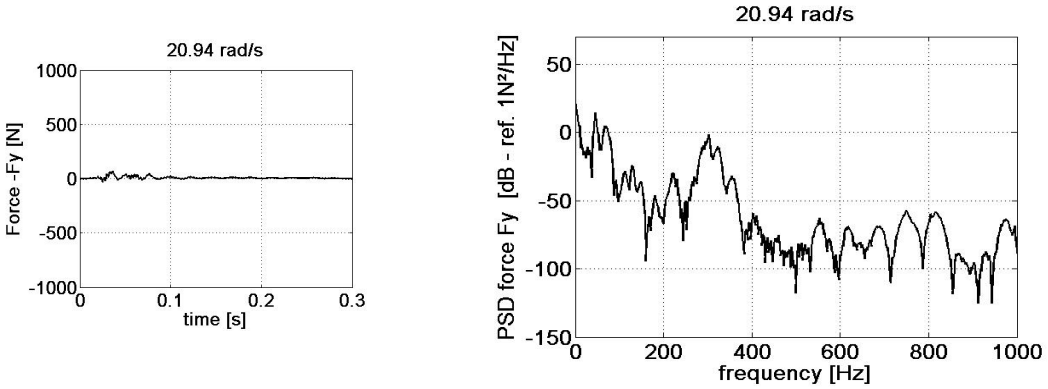

Fig. 4b: Lateral spindle force response

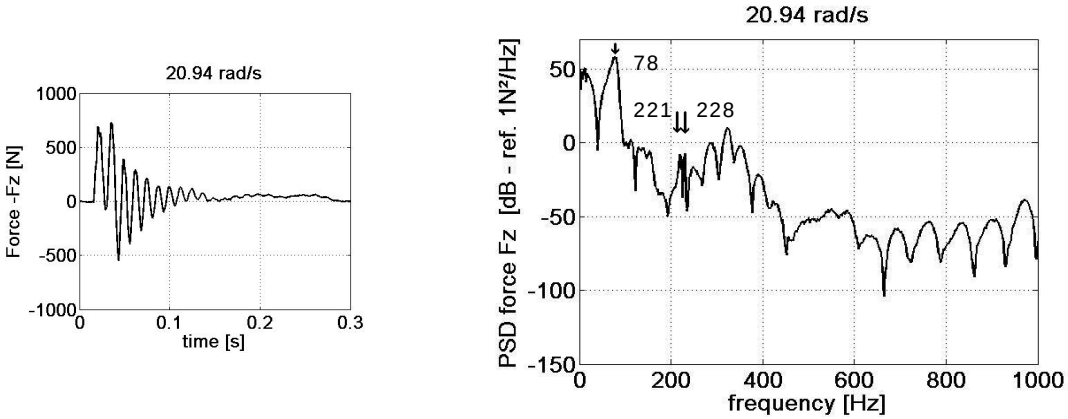

Fig. 4c: Vertical spindle force response

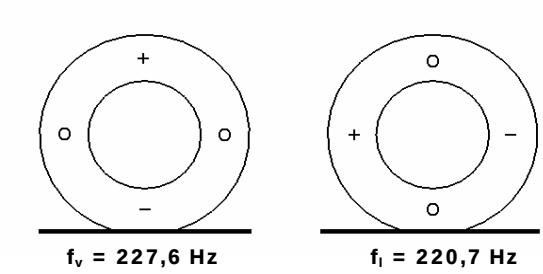

Fig. 5: Acoustic pressure distributions at the two deformed tire acoustic resonances. (+:max. pressure; - :min. pressure; o :zero pressure)

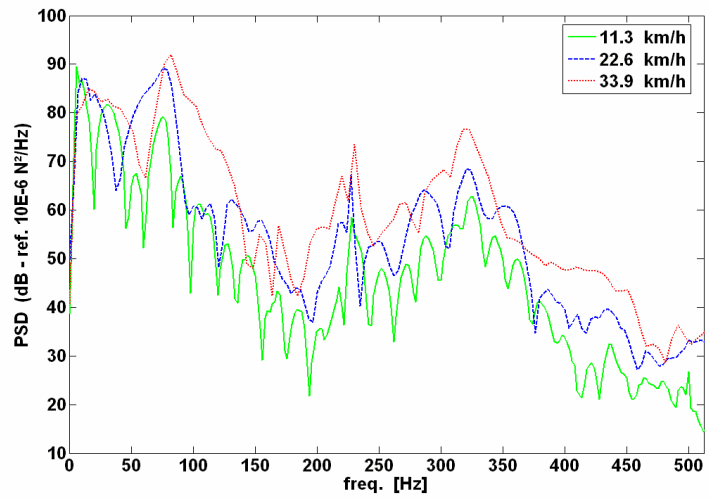

Fig. 6: Vertical spindle force spectrum at different driving speeds; 5mm high semi-circular cleat; inflation pressure 2.2 bar.

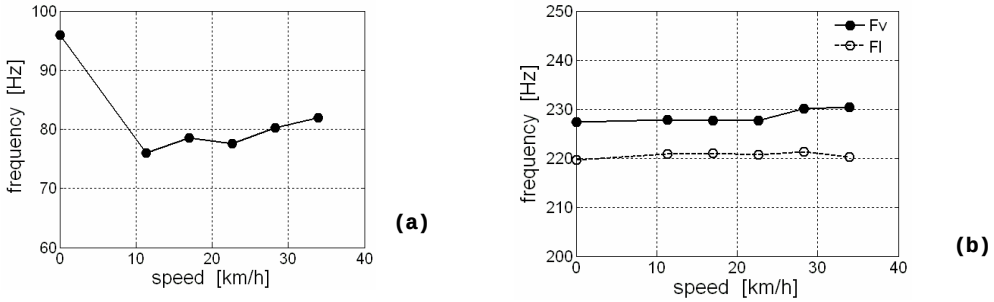

Fig. 7: (1,0) vertical resonance frequency (a) and acoustic resonance frequencies (b) as a function of rolling speed.

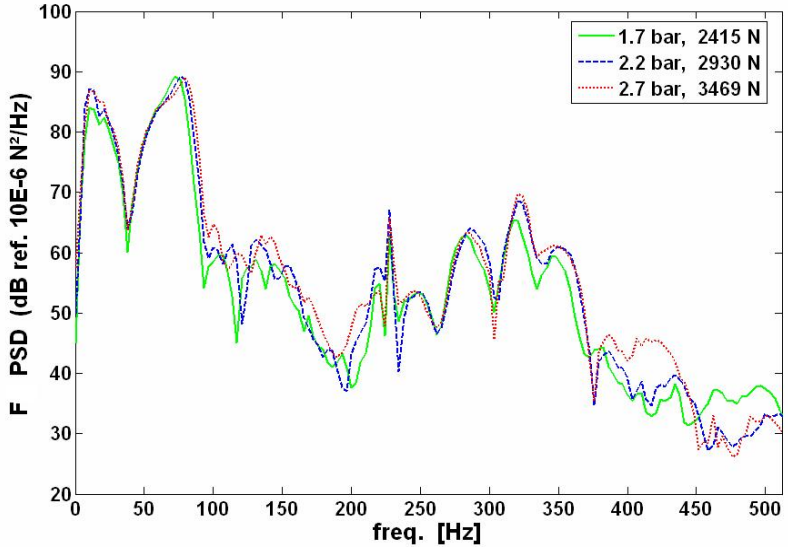

Fig. 8: Vertical spindle force spectrum at different inflation pressures; 5 mm high semi-circular cleat; driving speed 22.6 km/h.

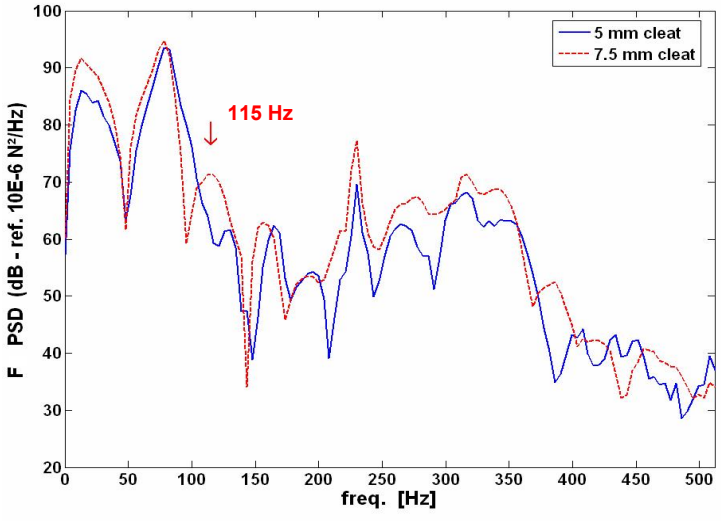

Fig. 9: Vertical spindle force spectrum for different cleat heights; driving speed 28.3 km/h; inflation pressure 2.2 bar.

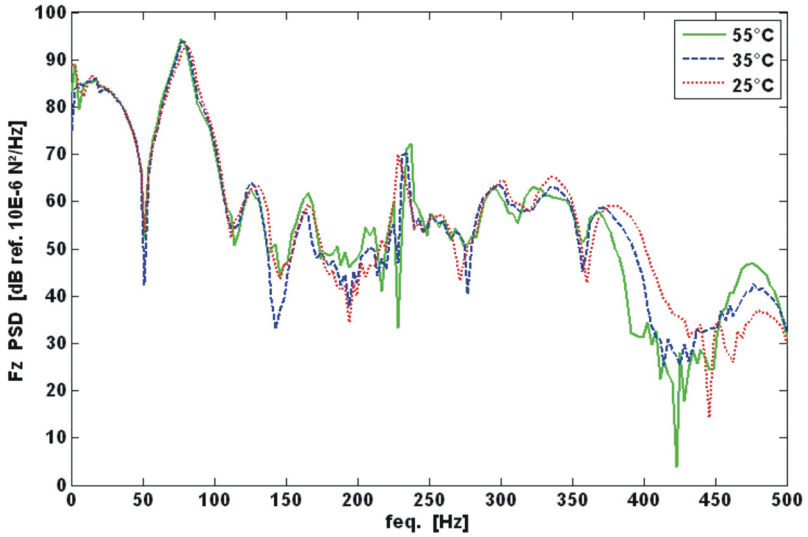

Fig. 10: Vertical spindle force spectrum for different tire temperatures; 5 mm high square cleat; driving speed 28.3 km/h.

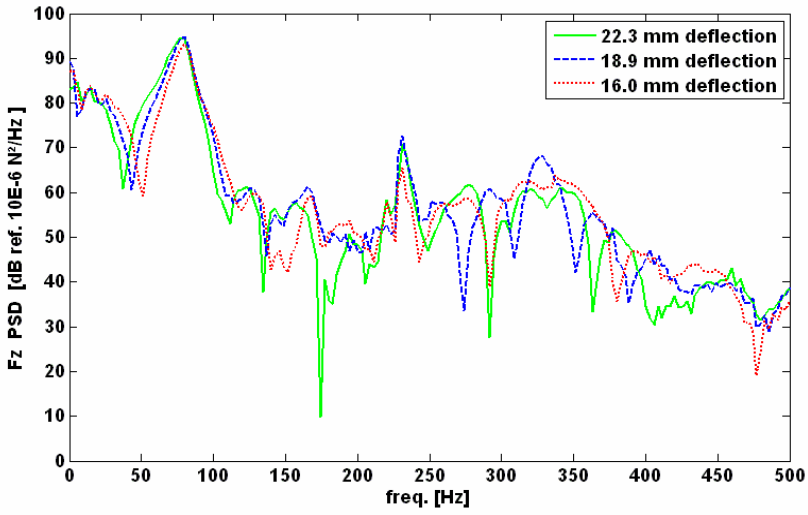

Fig. 11: Vertical spindle force spectrum for different static tire deflections; 5 mm high square cleat; driving speed 28.3 km/h.

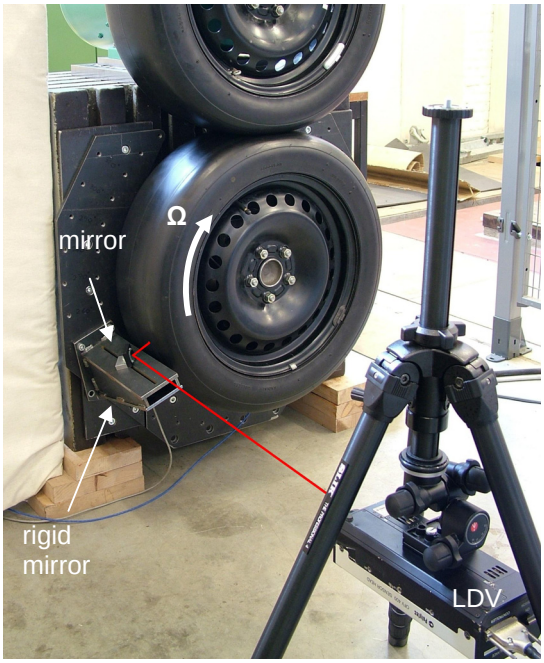

Fig. 12: Test setup for tire rolling vibration measurement by means of a Laser Doppler Vibrometer (red line show the path of the laser beam).

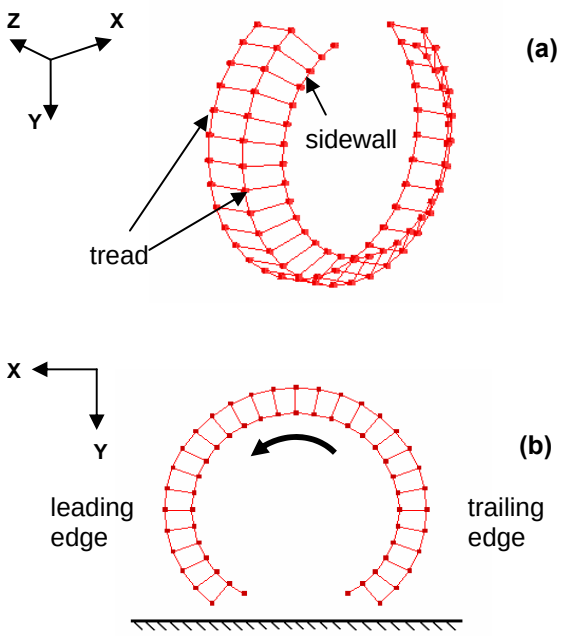

Fig. 13: (a) Measurement grid of the lower tire in the fixed reference frame.
(b) Measurement grid with indication of rotational direction.

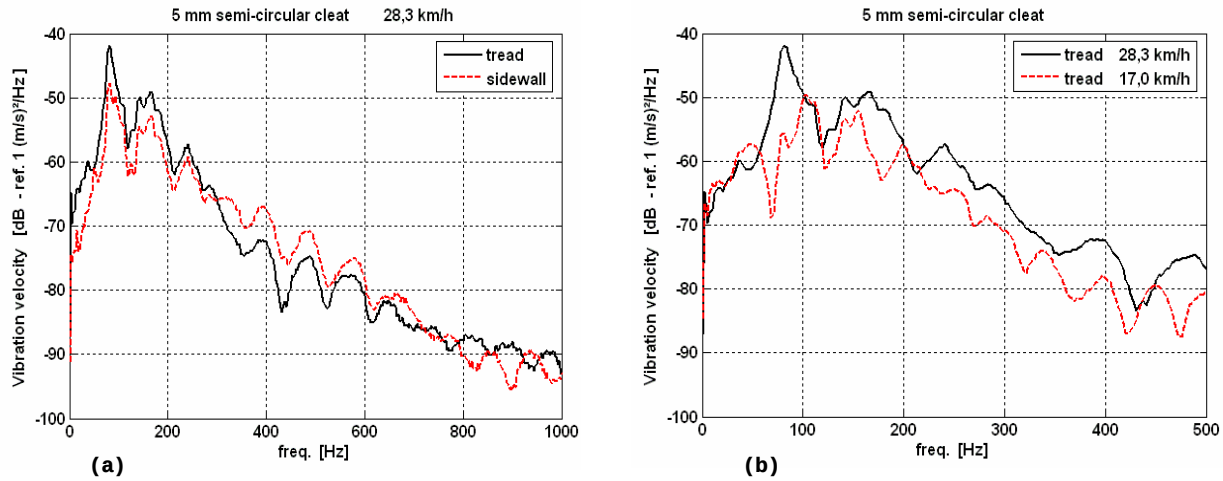

Fig. 14: (a) Averaged power spectral density of tread and sidewall vibration velocity at 28,3 km/h
(b) Averaged power spectral density of tread vibration velocity for two different rolling speeds

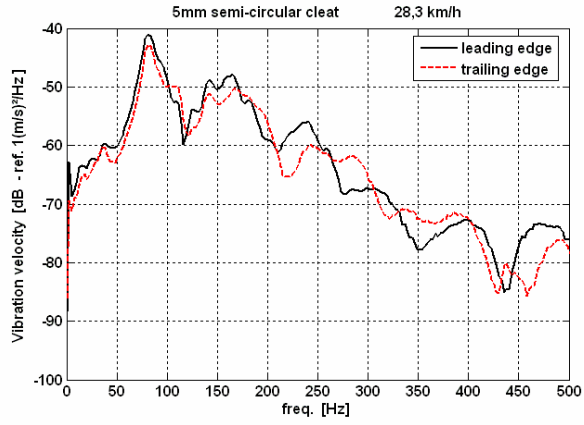

Fig. 15: Averaged power spectral density of tread vibration velocity at leading and trailing edge.

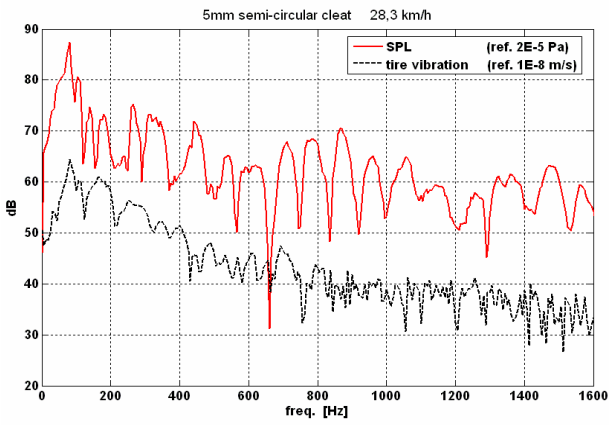

Fig. 17: Sound pressure level (SPL) and tire vibration spectrum measured at the same tread point.

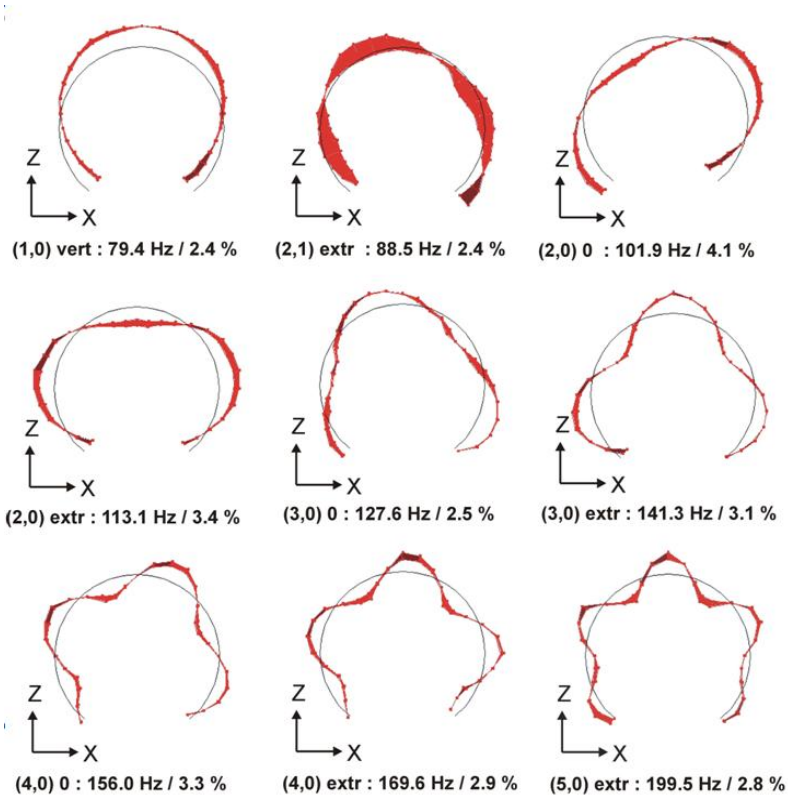

Fig. 16: Operational modal parameters of rolling tire (17km/h) excited by a semi-circular cleat of 5mm high.

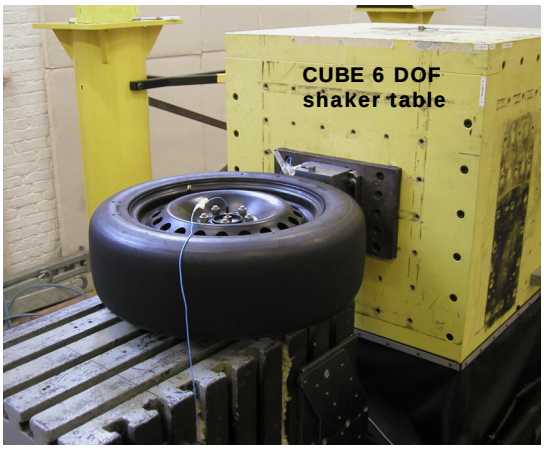

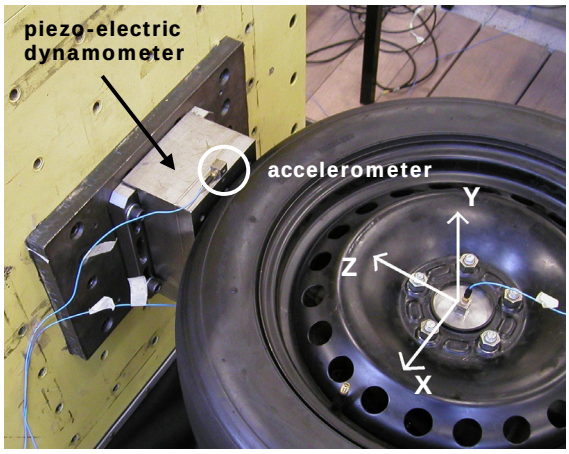

Fig. 18: Test setup for the dynamic stiffness measurement of a non-rotating tire.

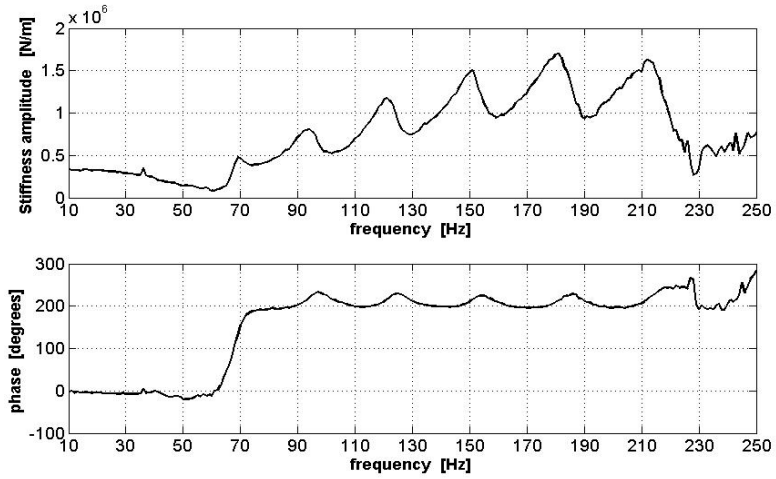

Fig. 19: Amplitude and phase of dynamic tire stiffness in the z-direction.

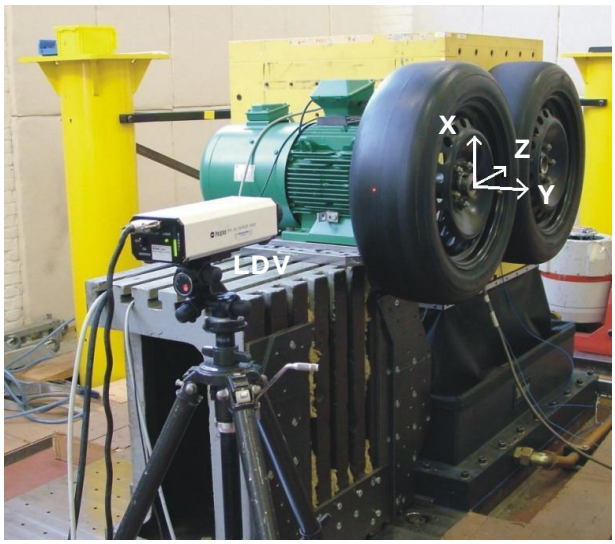

Fig. 20: Test setup for the operational modal analysis on a rotating tire by using shaker excitation.

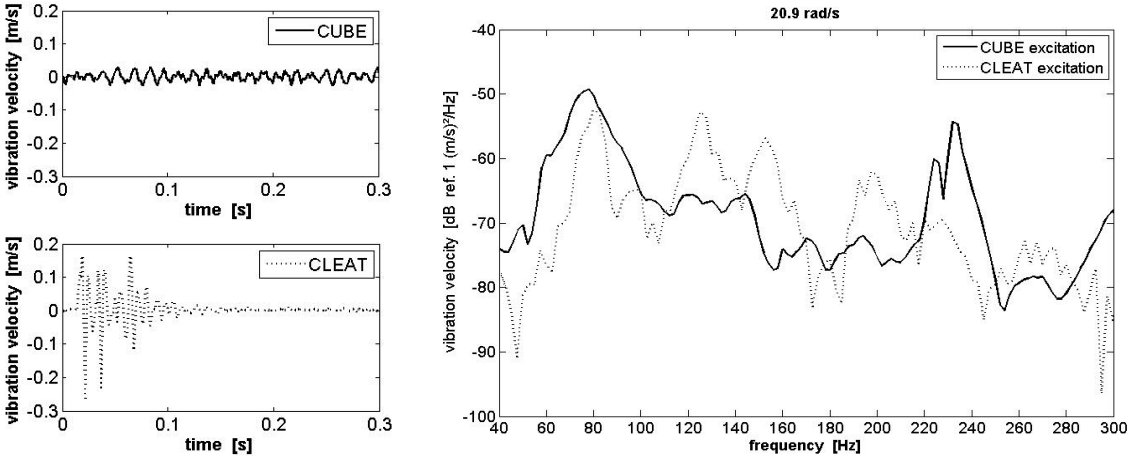

Fig. 21: Time signal and power spectral density of tread vibration velocity for CUBE shaker and cleat excitation.

	Frequency [Hz]			Damping [%]		
	0 km/h	**17,0 km/h**	**28,3 km/h**	**0 km/h**	**17,0 km/h**	**28,3 km/h**
(0,0) axial	49.45	45.95	*	2.09	2.84	*
(1,1) horiz	*	74.85	77.15	*	2.50	6.01
(1,1) vert	61.53	*	*	2.58	*	*
(1,0) horiz	108.51	*	*	1.53	*	*
(1,0) vert	95.82	79.6	81.83	3.93	2.90	4.34
(2,0) 0	*	102.79	102.98	*	2.16	3.02
(2,0) extr	125.69	113.73	113.94	2.93	2.64	3.66
(2,1) 0	131.43	95.65	96.09	3.21	2.04	3.41
(2,1) extr	103.59	89.12	91.29	2.80	1.65	2.79
(3,0) 0	142.10	129.00	124.09	3.33	2.57	2.60
(3,0) extr	156.53	141.68	139.33	2.82	2.21	3.87
(3,1) 0	189.69	*	*	0.65	*	*
(4,0) 0	171.83	155.34	151.76	2.91	2.22	2.62
(4,0) extr	187.40	171.26	167.52	2.57	1.95	3.29
(4,1) 0	222.72	*	*	2.47	*	*
(5,0) 0	204.47	184.79	182.70	2.51	2.05	3.71
(5,0) extr	*	199.29	199.88	*	2.46	1.50
(5,1) 0	254.78	*	*	3.48	*	*
acoust. horiz	220.07	223.25	*	0.34	1.74	*
acoust. vert	227.06	227.85	*	0.38	0.45	*

Table 1: Tire resonance frequencies at different rolling speeds, semi-circular cleat 7.5 mm (* indicates a not identified mode)